Liquid Crystals
Publication details, including instructions for authors and subscription information:
http://www.informaworld.com/smpp/title~content=t713926090

Synthesis and mesomorphic properties of 7-alkoxybezopyrano[2,3-c]pyrazol-3-one

Yan Li[a]; Xinbing Chen[a]; Pei Chen[a]; Zhongwei An[a]; Juan Li[a]
[a] Key Laboratory of Applied Surface and Colloid Chemistry (Shaanxi Normal University), Ministry of Education, School of Chemistry and Materials Science, Shaanxi Normal University, Xi'an, PR China

Online publication date: 10 December 2010

To cite this Article Li, Yan , Chen, Xinbing , Chen, Pei , An, Zhongwei and Li, Juan(2010) 'Synthesis and mesomorphic properties of 7-alkoxybezopyrano[2,3-c]pyrazol-3-one', Liquid Crystals, 37: 12, 1549 — 1557
To link to this Article: DOI: 10.1080/02678292.2010.527019
URL: http://dx.doi.org/10.1080/02678292.2010.527019

Liquid Crystals,
Vol. 37, No. 12, December 2010, 1549–1557

Taylor & Francis
Taylor & Francis Group

Synthesis and mesomorphic properties of 7-alkoxybezopyrano[2,3-c]pyrazol-3-one

Yan Li, Xinbing Chen*, Pei Chen, Zhongwei An and Juan Li

Key Laboratory of Applied Surface and Colloid Chemistry (Shaanxi Normal University), Ministry of Education, School of Chemistry and Materials Science, Shaanxi Normal University, Xi'an, PR China

(*Received 16 August 2010; final version received 22 September 2010*)

A new series of fused polyheterocyclic aromatic compounds, 7-alkoxybezopyrano[2,3-c]pyrazol-3-one (**C-*n*BPP**), were synthesised and characterised by infrared, ^{1}H-nuclear magnetic resonance (NMR), ^{13}C-NMR and two-dimensional ^{1}H-^{13}C cosy spectra. Their phase transition behaviour was investigated by differential scanning calorimetry and polarising optical microscopy. All of these compounds showed enantiotropic mesophases with temperature domains of 12–60°C and 22–69°C on heating and cooling processes for a carbon number of the alkoxy chain from 2 to 10. The effect of the length of the alkoxy chain on the mesomorphic properties was discussed. Comparison of **C-*n*BPP** and several kinds of coumarin derivatives indicated that the intermolecular hydrogen bonding acted as the driving force of the mesophase formation.

Keywords: mesomorphic phase; hydrogen bonding; bezopyrano[2,3-c]pyrazol-3-one

1. Introduction

Over the past few decades, the driving force of the mesophase formation has been a fundamental topic of study in the field of liquid crystal molecular engineering, in which the molecular shape is considered to be primary [1, 2]. It has been well documented that the thermotropic mesomorphase is basically dependent on the molecular architecture in which a slight change in the molecular geometry, such as rod-like [3, 4], disc-like [5–7], star-shaped [8, 9], U-shaped [10, 11], V-shaped [12] and T-shaped [13, 14], brings about a considerable change in its properties. Efforts focused on modification of existing molecules have proved this to be an effective method to obtain novel liquid crystals. Over many years a large number of heterocyclic units have been designed and prepared to substitute the benzene or naphthalene unit as the mesogenic core, such as 1,2,3-triazoles [15, 16], 1,3,4-oxadiazoles [17–20], flavone and isoflavone [21–23] and coumarin [24–26]. As core units in thermotropic liquid crystals, heterocycles have attracted more and more attention because the incorporation of heteroatoms (N, O and S, commonly introduced) can result in considerable changes in the corresponding mesophases due to their much larger polarity than carbon [27]. In particular, coumarin derivatives, which possess useful applications in different areas, have also been studied as mesogenic units based on their strong dipole moments.

Recently, a series of fused polyheterocyclic aromatic compounds derived from coumarin derivatives have been reported as potential biological active compounds [28], in which the bezopyrano[2,3-c]pyrazol-3-one (BPP) structure composed of coplanar π-conjugated polyheterocyclics has potential applications as the mesogenic unit in developing novel liquid crystal compounds due to its fused rings, heteroatoms and various active positions. However, to date there has been no report on BPP-based liquid crystal compounds.

With the aim of better understanding the structure–property correlations in liquid crystal compounds and to investigate the application feasibility of BPP-based compounds as liquid crystal, herein we have designed and synthesised a series of fused polyheterocyclic aromatic compounds, 7-alkoxybezopyrano[2, 3-c]pyrazol-3-one (**C-*n*BPP**) (Figure 1), where coumarin is fused with other heterocycles. All of these compounds have the same bezopyrano[2,3-c]pyrazol-3-one unit connected with an alkoxy chain group with carbon number from 2 to 10. The reason for the selection of bezopyrano[2,3 -c]pyrazol-3-one as both core unit and end group is that we want to study how the NH group in bezopyrano[2,3 -c]pyrazol-3-one affects their thermal behaviour. All of the compounds exhibit stable enantiotropic mesophases with temperature domains of 12–60°C and 22–69°C on heating and cooling processes. The effect of the length of the alkoxy chain on mesomorphic properties is discussed. To investigate the driving force of the mesophase formation, several kinds of coumarin derivatives, ethyl 7-alkoxycoumarin-3-carboxylate (**B-n**), 7-alkoxycoumarin-3-carboxylic acid (**D-n**) and 7-alkoxycoumarin (**E-n**), were prepared (Scheme 1) and their thermal behaviours are discussed.

*Corresponding author. Email: chenxinbing@snnu.edu.cn

ISSN 0267-8292 print/ISSN 1366-5855 online

DOI: 10.1080/02678292.2010.527019
http://www.informaworld.com

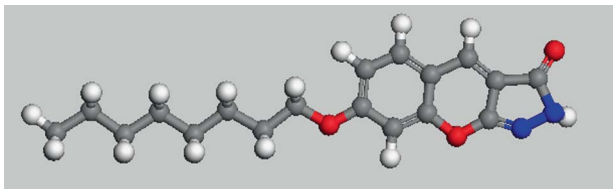

Figure 1. A molecular model of **C-*n*BPP** (n=8) containing fused rings (colour version online).

2. Results and discussion

2.1 Synthesis and characterisation

A synthetic route towards 7-alkoxybezopyrano[2,3-c] pyrazol-3-one (**C-*n*BPP**), a kind of fused polyheterocyclic aromatic compound, is illustrated in Scheme 1. 7-Hydroxycoumarin-3-carboxylate was obtained from 2,4-dihydroxybenzaldehyde and diethyl malonate by Knoevenagel condensation. Nucleophilic substitution of 7-hydroxycoumarin-3-carboxylate was accomplished with the corresponding bromoalkanes in the presence of anhydrous potassium carbonate. Then hydrazinolysis cyclocondensation of the prepared 7-alkoxycoumarin-3-carboxylate was carried out with hydrazine hydrate for several hours. As a result, compounds **C-*n*BPP** containing 2, 3, 4, 5, 6, 7, 8 and 10 carbon atoms were obtained with purities higher than 99% (gas chromatography (GC) and high-performance liquid chromatography (HPLC)) and overall yields of 22–28%.

The structures of the products and intermediates were characterised by mass spectrometry (MS), infrared (IR) and ^{1}H-nuclear magnetic resonance (NMR) spectra. From the IR data of compounds **C-*n*BPP**, the absorption band at 3430 cm^{-1} was assigned to the vibration of the NH group in the fused polyheterocyclic aromatic ring. Compared to compounds **B-n,** the vibrations of C=O were red-shifted from 1750 and 1701 cm^{-1} to 1630 and 1620 cm^{-1} for compounds **C-*n*BPP** due to p–π conjugation between C=O and NH, which overlapped with the characteristic absorption bands of C=N at 1620 cm^{-1}. Four kinds of protons appearing at 6.43–11.70 ppm in the ^{1}H-NMR spectra were assigned to the protons of the fused polyheterocyclic aromatic ring for compounds **C-*n*BPP**, in which a proton of the N–H bond appeared at 11.70 ppm. In the case of **C-5BPP**, further confirmation of the structure was performed by ^{13}C-NMR and two-dimensional (2D) ^{1}H-^{13}C cosy spectra measurements. The 2D ^{1}H-^{13}C cosy spectra of **C-5BPP** are shown in Figure 2. With the aid of the proton spectrum assignments, protonated carbons were readily assigned. The carbon resonances at 100.6 and 106.9 ppm were found to be correlated with the proton peak at 6.48 ppm, while non-protonated carbons at 100.9, 160.7 and 162.4 ppm were assigned according to the 2D ^{1}H-^{13}C Heteronuclear Multiple Bond Correlation (HMBC) cosy spectra. Note that the ^{13}C-NMR spectrum showed only 12 carbon resonance peaks which is less than 15; the lack of carbon resonances could be explained reasonably by the overlaps of some carbon resonances due to their similar chemical environments based on the 2D ^{1}H-^{13}C HMBC and Heteronuclear Single Quantum Coherence (HSQC) cosy spectra. All of these results, including IR, ^{1}H-NMR, ^{13}C-NMR and 2D ^{1}H-^{13}C cosy spectra data, provide clear evidence that **C-5BPP** is consistent with the proposed structure.

2.2 Mesomorphic properties

Mesomorphic properties for compounds **C-*n*BPP** were determined by differential scanning calorimetry (DSC) measurements and polarising optical microscopy (POM) observations. Phase identification was made by comparing the observed textures with those reported in the literature. DSC curves obtained under the same conditions overlapped with each other, indicating that the reproducibility of the measurements was satisfactory. The phase transition temperatures reported in this paper were the peak values of the transitions on the DSC curves. The phase transition temperatures, the associate enthalpy changes and the mesophase textures of **C-*n*BPP** are summarised in Table 1. Clear-cut transition temperatures and textures could be obtained from the DSC curves and POM observations for all of the compounds, and they were in good agreement with each other for the multiple heating/cooling cycles.

As seen in Table 1, all of these compounds exhibited enantiotropic mesophases with temperature domains of 12–60°C and 26–63°C in the heating and cooling processes for carbon numbers of the alkoxy chain from 2 to 10. Compound **C-5BPP** showed endotherms at 150.0°C and 177.6°C corresponding to the melting and mesophase–isotropic phase transition phenomena on the heating process, as shown in Figure 3(a). The texture of the mesophase formed is shown in Figure 3(b), which showed a typical schlieren texture under POM observation. Therefore, the mesophase was assigned to be a nematic (N) phase. The molten **C-5BPP** showed a small exotherm at 175.5°C, a slightly higher exotherm at 148.2°C and a large exotherm at 108.1°C due to the phase transition during the cooling process. The textures formed are shown in Figures 3(c) and 3(d); the first mesophase displayed a cross-like droplet texture (N phase) and the second mesophase below N phase was assigned to be a smectic A (SmA) phase due to its fan-shaped characteristic texture. **C-4BPP**, **C-6BPP**

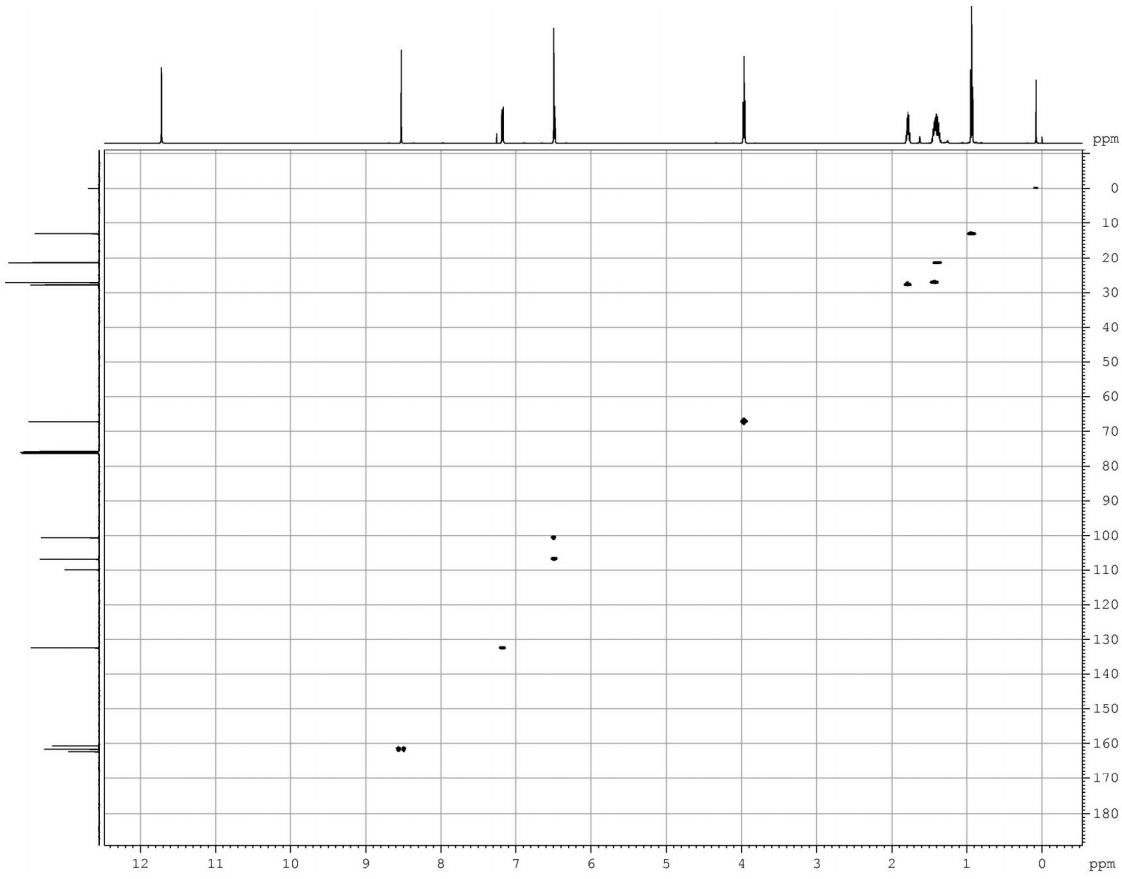

Figure 2. 2D ^{1}H-^{13}C cosy spectra of **C-5BPP**.

Table 1. Types of phase transitions, temperatures and corresponding enthalpies obtained by polarising optical microscopy and differential scanning calorimetry methods for compounds **C-*n*BPP**.

		Transition temperature/°C (enthalpy change/kJ mol^{-1})	
Compounds	*n*	Heating process	Cooling process
C-2BPP	2	Cr 190.0 (22.5) N 209.0 (0.6) I	I 207.0 (−0.7) N 180.7 (−23) Cr
C-3BPP	3	Cr 175.1 (35.6) N 186.6 (0.2) I	I 180.7 (−0.5) N 159.1 (−27.7) Cr
C-4BPP	4	Cr 155.3 (27.1) SmA 162.9 (1.6) N 190.6 (0.7) I	I 188.0 (−0.8) N 127.2 (−0.8) SmA 119.4 (−25.2) Cr
C-5BPP	5	Cr 150.0 (26.4) N 177.6 (0.8) I	I 175.5 (−0.8) N 148.2 (-1.5) SmA 108.1 (-23.4) Cr
C-6BPP	6	Cr 132.5 (24.3) SmA 163.5 (1.7) N 178.9 (0.9) I	I 176.6 (−1.1) N 160.8 (−1.3) SmA 107.4 (−22.5) Cr
C-7BPP	7	Cr 126.0 (25.0) SmA 167.5 (2.5) N 172.0 (0.9) I	I 169.2 (−1.4) N 164.4 (−2.4) SmA 104.1 (−24.5) Cr
C-8BPP	8	Cr 111.2 (20.1) SmA 168.5 (4.0) I	I 165.1 (−4.0) SmA 96.9 (−19.9) Cr
C-10BPP	10	Cr_1 83.9 (6.2) Cr_2 106.0 (13.7) SmA 165.5 (3.9) I	I 162.5 (−3.8) SmA 99.8 (−14.4) Cr

Notes: Cr_1 and Cr_2: crystal; N: nematic mesophase; SmA: smectic A mesophase; I: isotropic liquid.

and **C-7BPP** displayed enantiotropic phase sequences of Cr–SmA–N–I and I–N–SmA–Cr in the heating and cooling processes, respectively, while compound **C-5BPP** exhibited the sequences Cr–N–I (heating) and I–N–SmA–Cr (cooling) as described above. It was found that compound **C-2BPP** only exhibited an enantiotropic N mesophase, which was assigned from the typical schlieren texture as shown in Figure 4(a), whereas **C-10BPP** with the longest terminal alkoxy chain exhibited a crystal transition at 83.9°C followed by an enantiotropic SmA mesophase identified by the fan-shaped texture (Figure 4(b)).

2.3 The effect of alkoxy chain on liquid crystalline properties

Figure 5 plots the transition temperatures of compounds **C-*n*BPP** as a function of the number of

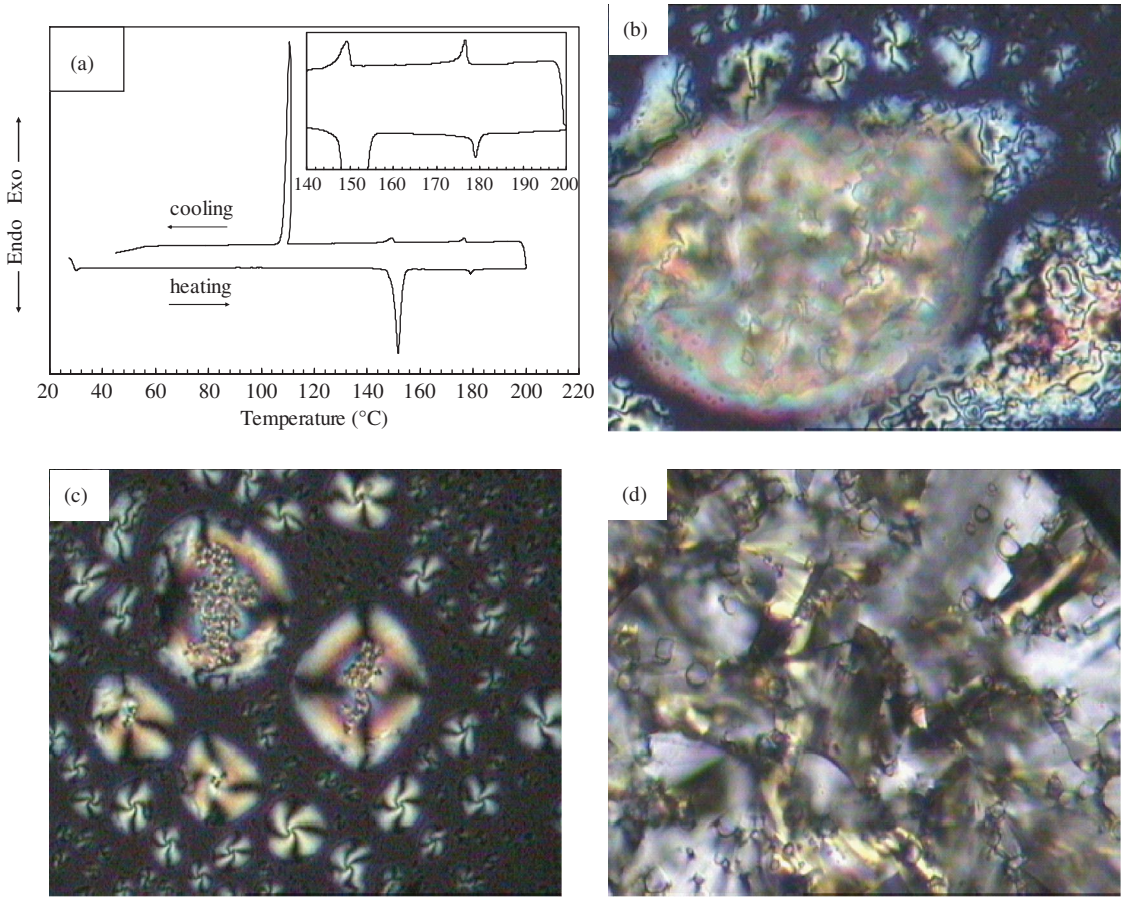

Figure 3. DSC traces and photomicrographs (×200) of **C-5BPP**. (a) DSC traces at a scanning rate of 5°C/min; (b) a schlieren texture of the N mesophase at 170°C on heating; (c) a cross-like droplet texture of the N mesophase at 170°C on cooling; (d) a fan-shaped texture of the smectic mesophase at 135°C on cooling (colour version online).

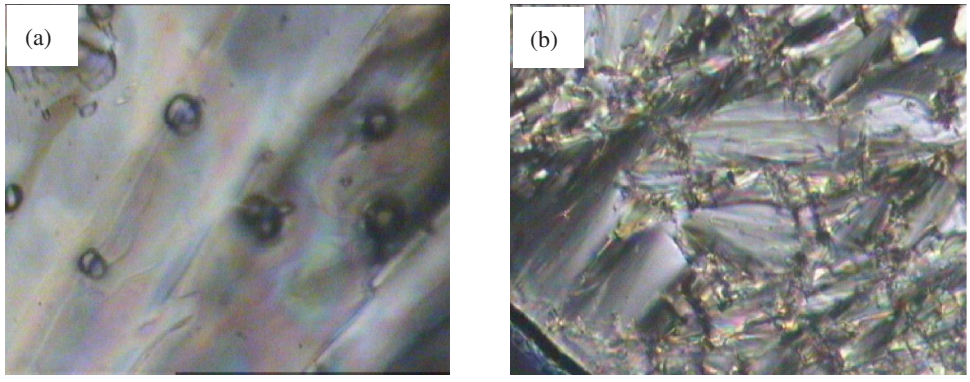

Figure 4. Photomicrographs (×200) of (a) a schlieren N texture of **C-2BPP** at 200°C on heating; (b) a fan-shaped smectic texture of **C-10BPP** at 150°C on heating (colour version online).

methylenic units (*n*) in the alkoxy chain in the heating process. It is clear that the length of the alkoxy chain influenced not only the nature of the mesophases but also the mesomorphic temperature ranges. Generally, an increase in terminal length often results in an enhanced induced-dipole–induced-dipole interaction between the terminal chains, leading to the formation of a more ordered smectic mesophase in rod-like mesogens. Consequently, compounds **C-*n*BPP** with shorter terminal chain (*n*=2, 3) showed a N phase, while the analogues with longer terminal chain (*n*=4–7) exhibited a SmA phase as well as a N phase, and the other

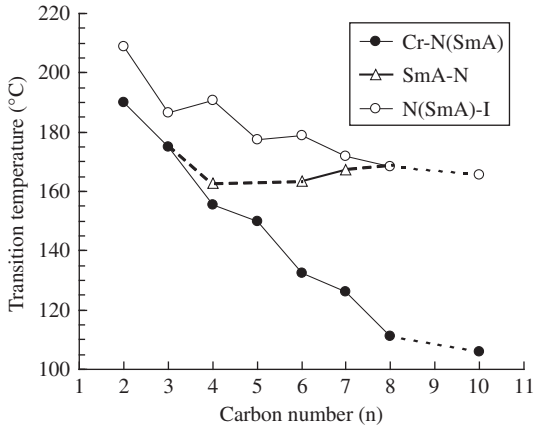

Figure 5. Transition behaviour of the compounds **C-*n*BPP**: dependence of the transition temperatures on the number (*n*) of methylene units of the alkoxy chain.

analogues only displayed a smectic phase due to the much longer alkoxy chain (*n*=8, 10). As shown in Figure 5, the melting temperature points of **C-*n*BPP** decreased smoothly with ascending homologues. The N–isotropic (I) liquid or the SmA–I liquid transition temperature points exhibited the same decreasing tendency, as well as a clear odd–even effect with the increase of the carbon numbers (*n*). It was noted that the increase of the alkoxy chain length from 2 to 10 resulted in a gradual increase and then a decrease of the range of the N phase and an increase of the range of the SmA phase, suggesting that as the chains get longer the induced-dipole–induced-dipole interaction between the terminal chains becomes stronger. As a result, the elongation of the terminal alkoxy chain produced an enhancement of the mesomorphic temperature ranges of **C-*n*BPP** from 12 to 60°C in the heating process and from 22 to 69°C in the cooling process.

2.4 The driving force of the mesophase formation

Note that **C-2BPP**, only containing an ethoxy chain, possesses a length-to-width ratio of about 2.5, which is smaller than the thermotropic liquid crystal length-to-width ratio of 3 [29]. **C-2BPP** showed N mesophase domains of 19°C and 26°C in the heating and cooling processes. It was interesting to investigate the driving force of the mesophase formation for compounds **C-*n*BPP**. For comparison, several kinds of analogous coumarin derivatives were prepared and DSC measurements performed. The phase transition temperatures of **B-*n***, **D-*n*** and **E-*n*** are summarised in Table 2. Compared with **C-*n*BPP**, it was obvious that the compounds **B-*n***, **D-*n*** and **E-*n*** displayed no mesomorphic prosperity, indicating that a slight difference in core units has a very different effect on the thermal behaviour. Although the core units in **B-*n*** and **E-*n*** had been utilised as part of the mesogen units [24–26], they were not enough to act as mesogen units by themselves in the present cases. The compounds **D-*n*** possessed a carboxyl acid group in their core unit, which was helpful in the formation of hydrogen bonding interactions and thus stabilised the possible mesophase. It is well known that aromatic carboxyl acid [30] shows a mesophase due to the formation of a dimer in which the intermolecular hydrogen bonding along the molecular long axis is utilised to form a new and elongated mesogenic unit to achieve and stabilise the liquid crystal phase. Unfortunately, **D-*n*** exhibited no liquid crystal phase, indicating the non-existence of the dimer formed by the intermolecular hydrogen bonding in the compound. This was attributed to the easy formation of a six-membraned ring in compounds **D-*n*** by the intramolecular hydrogen bonding, as shown in Figure 6(a). For compounds **C-*n*BPP**, the dimer could be formed by the intermolecular hydrogen bonding interaction due to the easy formation of an eight-membraned ring rather than an intramolecular four-membraned ring, as shown in Figure 6(b). The dimer elongated and formed a new mesogenic unit, and thus the length-to-width ratio was large enough to generate a mesophase, similar to the case in aromatic carboxyl acid [30]. Therefore, the intermolecular hydrogen bonding was considered to be the driving force of the mesophase formation in the case of **C-*n*BPP**.

Table 2. Transition temperatures and the associated enthalpy changes of the compounds **C-*n*BPP**, **B-*n***, **D-*n*** and **E-*n*** (*n*=5, 8).

Compounds	*n*	Transition temperature/°C (enthalpy change/kJ mol^{-1})	Compounds	*n*	Transition temperature/°C (enthalpy change/kJ mol^{-1})
C-5BPP	5	Cr 150.0 (26.4) N 177.6 (0.8) I	**C-8BPP**	8	Cr 111.2 (20.1) SmA 168.5 (4.0) I
B-5	5	Cr 94.1 (32.7) I	**B-8**	8	Cr 79.9 (34.3) I
D-5	5	Cr 153.0 (37.7) I	**D-8**	8	Cr 140.2 (42.4) I
E-5	5	Cr 30.8 (n.d.) I	**E-8**	8	Cr 47.9 (36.7) I

Notes: Cr: crystal; N: nematic mesophase; SmA: smectic A mesophase; I: isotropic liquid; n.d.: no data available.

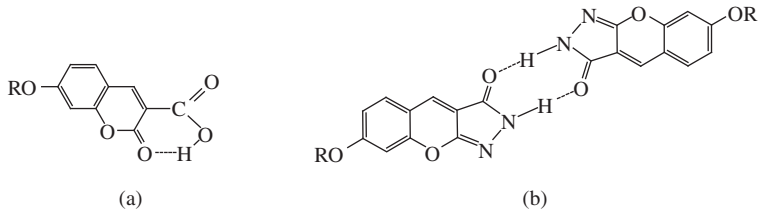

Figure 6. The hydrogen bonding structures: (a) intramolecular hydrogen bonding in **D-*n*** and (b) intermolecular hydrogen bonding in **C-*n*BPP**.

3. Conclusions

In summary, liquid crystal compounds derived from a unique fused polyheterocyclic aromatic mesogenic core were synthesised and characterised. All of them exhibited enantiotropic mesomorphic phases with temperature domains of 12–60°C and 22–69°C in the heating and cooling processes for carbon numbers of the alkoxy chain from 2 to 10. The melting points decreased on ascending the homologues, while the N–I or SmA–I transition temperatures showed a clear odd–even effect with the increase of the carbon numbers (*n*). Moreover, the intermolecular hydrogen bonding was considered to be the driving force of the mesophase formation.

4. Experimental

4.1 Materials

2,4-Dihydroxybenzaldehyde, bromoalkanes, piperidine, 7-hydroxycoumarin and hydrazine hydrate were purchased from Aladdin-reagent Co. and used as received. Acetic acid, absolute ethanol, diethylmalonate, N,N-dimethylformamide (DMF), tetrabutyl ammonium bromide (TBAB), sodium hydroxide, CH_2Cl_2, potassium iodide and anhydrous potassium carbonate were purchased from Sinopharm Chemical Reagent Co. and anhydrous potassium carbonate was dried at 150°C in vacuum prior to use.

4.2 Characterisation and measurements

The structures of the final products and intermediates were confirmed by a variety of spectral methods. IR spectra were recorded on a Nicolet Avatar360E spectrometer. ^{1}H-NMR, ^{13}C-NMR and 2D ^{1}H-^{13}C cosy spectra, with tetramethylsilane (TMS) as internal standard, were recorded on a Bruker AV 300 (300 MHz) instrument. The mass spectra were obtained by GC/MS Thermo DSQ II with m/z 50 to 650. The phase transition temperatures of the target compounds were measured by DSC (Shimatsu DSC-60) in nitrogen at heating and cooling rates of 5°C/min, and POM (Changfang XPN-300E with a heating stage and a control unit).

4.3 Synthesis

The compounds were prepared through a three-step reaction, namely Knoevenagel condensation, nucleophilic substitution followed by hydrazinolysis cyclocondensation, as shown in Scheme 1.

4.3.1 Synthesis of ethyl 7-hydroxycoumarin-3-carboxylate (**A**)

To a 100 mL, three-neck, round-bottom flask equipped with an overhead stirrer and condenser, 0.50 g of 2,4-dihydroxybenzaldehyde (3.6 mmol), 0.64 g of diethyl malonate (0.61 mL, 4.0 mmol, 10 mol% excess)

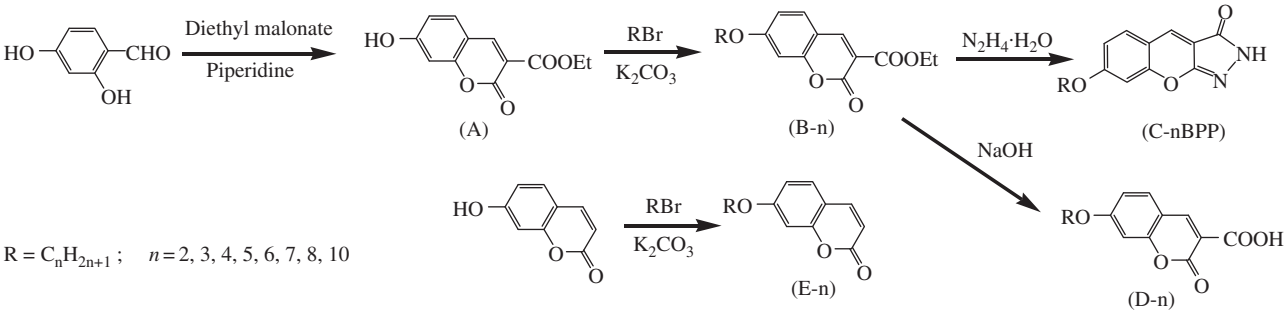

Scheme 1. Synthetic routes of **C-*n*BPP**, **B-*n***, **D-*n*** and **E-*n***.

and 20 mL of absolute ethanol were added. The mixture was heated with stirring until dissolution occurred. Then 0.34 g of piperidine (0.4 mL, 4.0 mmol) was added and the resulting solution was refluxed for 6 h; on cooling a yellow crystalline solid formed. Crystals of ethyl 7-hydroxycoumarin-3-carboxylate (1) were isolated by filtration and washed with cold ethanol. The solid was recrystallised from ethanol (75%), filtered and washed with cold ethanol (75%) again. The crystals were dried in a vacuum oven at 50°C for 24 h. The yield was 50% with a GC purity of more than 99%.

Melting point (m.p.) 172–174°C (literature 174–177°C [31]). ^{1}H-NMR (300 MHz, DMSO, TMS): δ (ppm) 8.67 (s, 1H); 7.74 (d, 1H, J=8.5 Hz); 6.85 (d, 1H, J=8.5 Hz); 6.73 (s, 1H); 4.25 (q, 2H, J=6.9 Hz); 1.29 (t, 3H, J=6.9 Hz). MS m/z (relative intensity): 234 (M^+, 36), 189 (99), 162 (100), 134 (33), 105 (37).

*4.3.2 Synthesis of ethyl 7-alkoxycoumarin-3-carboxylate (***B-*n***)***

Ethyl 7-alkoxycoumarin-3-carboxylate (**B-*n***), where *n* in parentheses refers to the carbon number of the alkoxy group was prepared. As an example, the preparation procedure of ethyl 7-pentyloxycoumarin-3-carboxylate (**B-5**) is described below.

To a 250 mL, three-neck, round-bottom flask equipped with an overhead stirrer and condenser, 2.34 g of ethyl 7-hydroxycoumarin-3-carboxylate (10 mmol), 60 mL of N,N-dimethylformamide, 3.45 g of anhydrous potassium carbonate, 0.35 g of TBAB and 1 g of potassium iodide were added. The mixture was heated at 80°C with stirring until a colour change from green to yellow occurred. Then 2.27 g of pentylbromide (15 mmol) in 25 mL of DMF was added slowly with stirring at 80°C. The reaction mixture was stirred at 80°C for 16 h. After the mixture was cooled to room temperature, it was filtrated. The filtrate was slowly poured into water. The resulting precipitate was thoroughly washed with water to neutral and then was recrystallised from ethanol.

Yield 2.71 g of white crystal (m.p. 94°C, yield of 89%). ^{1}H-NMR (300 MHz, $CDCl_3$, TMS): δ (ppm) 8.51 (s, 1H); 7.50 (d, 1H, J=8.6 Hz); 6.88 (d, 1H, J=8.6 Hz); 6.79 (s, 1H); 4.40 (q, 2H, J=7.0 Hz); 4.04 (t, 2H, J=6.3 Hz); 1.78–1.93 (m, 2H); 1.33–1.51 (m, 7H); 0.95 (t, 3H, J=6.6 Hz). IR (KBr, pellet, cm^{-1}): 3083, 2960, 2925, 2858, 1752, 1701, 1603, 1554, 1212, 1111, 1024, 974, 852. MS m/z (rel. int.): 304 (M^+, 16), 189 (38), 162 (100), 134 (12), 105 (22), 76 (8), 71 (5).

*4.3.3 Synthesis of 7-alkoxybezopyrano[2,3-c] pyrazol-3-one (***C-*n***BPP***)*

7-Alkoxybezopyrano[2,3-c]pyrazol-3-one (**C-*n*BPP**), where *n* in parentheses refers to the carbon number of the alkoxy group, was prepared through hydrazinolysis cyclocondensation. As an example, the preparation procedure of 7-pentyloxybezopyrano[2,3-c]pyrazol-3-one (**C-5BPP**) is described below.

To a 100 mL, three-neck, round-bottom flask equipped with an overhead stirrer and condenser, 0.61 g of **B-5** (2 mmol), 15 mL of absolute ethanol and 0.6 mL of hydrazine hydrate (85%) were added. The reaction mixture was stirred at reflux for 2 h. Then several drops of hydrochloric acid were added into the mixture to adjust the PH value below 3. The resulting mixture was stirred for another 1.5 h and transferred to a separatory funnel with 60 mL of CH_2Cl_2. The organic layer was washed several times with water to neutral and dried over anhydrous sodium sulphate. The solvent was removed under reduced pressure and the residue was purified by column chromatography on silica gel using CH_2Cl_2 as eluent.

The yield was 58% of pale yellow crystals. M.p. 150°C. ^{1}H-NMR (300 MHz, $CDCl_3$, TMS): δ (ppm) 11.72 (s, 1H); 8.53 (s, 1H); 7.12 (d, 1H, J=9.2 Hz); 6.38–6.45 (m, 2H); 3.91 (t, 2H, J=6.4 Hz); 1.66–1.77 (m, 2H); 1.33–1.36 (m, 4H); 0.86 (t, 3H, J=6.4 Hz). ^{13}C-NMR (300 MHz, $CDCl_3$, TMS): δ (ppm) 162.4, 161.7, 160.7, 132.4, 109.9, 106.9, 100.6, 67.2, 27.7, 27.1, 21.4, 13.0. IR (KBr, pellet, cm^{-1}): 3420 (NH), 2943, 2864, 1633 (C=O), 1621 (C=O and C=N), 1566, 1378, 1277, 1189, 1110, 975, 845, 800.

C-2BPP: The yield was 60% of pale yellow crystals. M.p. 190°C. ^{1}H-NMR (300 MHz, $CDCl_3$, TMS): δ (ppm) 11.66 (s, 1H); 8.49 (s, 1H); 7.12 (d, 1H, J=8.8 Hz); 6.39–6.47 (m, 2H); 3.99 (q, 2H, J=6.0 Hz); 1.36 (t, 3H, J=6.3 Hz). IR (KBr, pellet, cm^{-1}): 3431 (NH), 3077, 2967, 1638 (C=O), 1620 (C=O and C=N), 1566, 1384, 1269, 1188, 1107, 1029, 806.

C-3BPP: The yield was 63% of pale yellow crystals. M.p. 175°C. ^{1}H-NMR (300 MHz, $CDCl_3$, TMS): δ (ppm) 11.66 (s, 1H); 8.49 (s, 1H); 7.12 (d, 1H, J=8.7 Hz); 6.37–6.46 (m, 2H); 3.87 (t, 2H, J=6.3 Hz); 1.72–1.78 (m, 2H); 0.97 (t, 3H, J=7.1 Hz). IR (KBr, pellet, cm^{-1}): 3438 (NH), 2935, 2873, 1630 (C=O), 1616 (C=O and C=N), 1566, 1506, 1463, 1375, 1276, 1185, 1108, 1010, 973, 824, 765.

C-4BPP: The yield was 55% of pale yellow crystals. M.p. 155°C. ^{1}H-NMR (300 MHz, $CDCl_3$, TMS): δ (ppm) 11.65 (s, 1H); 8.46 (s, 1H); 7.11 (d, 1H, J=8.8 Hz);

6.37–6.45 (m, 2H); 3.90 (t, 2H, J=6.2 Hz); 1.60–1.77 (m, 2H); 1.33–1.48 (m, 2H); 0.90 (t, 3H, J=7.2 Hz). IR (KBr, pellet, cm^{-1}): 3423 (NH), 2954, 2926, 2866, 1635 (C=O), 1621 (C=O and C=N), 1567, 1506, 1379, 1279, 1213, 1188, 1112, 1064, 963, 842, 805.

C-6BPP: The yield was 58% of pale yellow crystals. M.p. 132°C. ^{1}H-NMR (300 MHz, $CDCl_3$, TMS): δ (ppm) 11.73 (s, 1H); 8.55 (s, 1H); 7.19 (d, 1H, J=8.6 Hz); 6.46–6.54 (m, 2H); 3.98 (t, 2H, J=6.0 Hz); 1.72–1.85 (m, 2H); 1.27–1.52 (m, 6H); 0.91 (t, 3H, J=6.0 Hz). IR (KBr, pellet, cm^{-1}): 3432 (NH), 2961, 2936, 2870, 2855, 1636 (C=O), 1621 (C=O and C=N), 1566, 1506, 1377, 1279, 1214, 1188, 1113, 999, 805.

C-7BPP: The yield was 52% of pale yellow crystals. M.p. 126°C. ^{1}H-NMR (300 MHz, $CDCl_3$, TMS): δ (ppm) 11.73 (s, 1H); 8.57 (s, 1H); 7.20 (d, 1H, J=9.1 Hz); 6.47–6.54 (m, 2H); 3.99 (t, 2H, J=6.3 Hz); 1.73–1.85 (m, 2H); 1.25–1.49 (m, 8H); 0.90 (t, 3H, J=6.0 Hz). IR (KBr, pellet, cm^{-1}): 3449 (NH), 2946, 2920, 2870, 2853, 1640 (C=O), 1627 (C=O and C=N), 1565, 1513, 1297, 1223, 1169, 1139, 1014, 959, 856.

C-8BPP: The yield was 53% of pale yellow crystals. M.p. 111°C. ^{1}H-NMR (300 MHz, $CDCl_3$, TMS): δ (ppm) 11.73 (s, 1H); 8.54 (s, 1H); 7.19 (d, 1H, J=9.0 Hz); 6.46–6.53 (m, 2H); 3.97 (t, 2H, J=6.4 Hz); 1.72–1.85 (m, 2H); 1.22–1.50 (m, 10H); 0.89 (t, 3H, J=6.3 Hz). IR (KBr, pellet, cm^{-1}): 3461 (NH), 2953, 2918, 2849, 1640 (C=O), 1628 (C=O and C=N), 1610, 1566, 1502, 1294, 1220, 1176, 1129, 1026, 963, 869.

C-10BPP: The yield was 50% of pale yellow crystals. M.p. 106°C. ^{1}H-NMR (300 MHz, $CDCl_3$, TMS): δ (ppm) 11.73 (s, 1H); 8.56 (s, 1H); 7.20 (d, 1H, J=9.2 Hz); 6.48–6.52 (m, 2H); 3.98 (t, 2H, J=6.5 Hz); 1.73–1.84 (m, 2H); 1.19–1.51 (m, 14H); 0.88 (t, 3H, J=6.8 Hz). IR (KBr, pellet, cm^{-1}): 3429 (NH), 3067, 2946, 2920, 2848, 1645 (C=O), 1633 (C=O and C=N), 1564, 1511, 1463, 1352, 1295, 1220, 1169, 1134, 853, 786.

*4.3.4 Synthesis of 7-alkoxycoumarin-3-carboxylic acid (***D-*n*)*

As an example, the preparation procedure of 7-pentyloxycoumarin-3-carboxylic acid (**D-5**) is described below.

To a 100 mL, three-neck, round-bottom flask equipped with an overhead stirrer and condenser, 0.91 g of **B-5** (3 mmol) and 30 mL of ethanol were added. The mixture was heated with stirring until dissolution occurred. Then 16.5 mL of aqueous sodium hydroxide (0.5M) was added slowly to keep a mild reflux. After addition, the reaction mixture was stirred at reflux for 30 min. After the mixture was cooled to room temperature, it was acidified with hydrochloric acid to a PH value of below 3. The obtained precipitate was recrystallised from ethanol.

The yield was 75% of white crystals. M.p. 153°C. ^{1}H-NMR (300 MHz, $CDCl_3$, TMS): δ (ppm) 12.23 (s, 1H); 8.85 (s, 1H); 7.64 (d, 1H, J=8.8 Hz); 7.01 (d, 1H, J=8.8 Hz); 6.91 (s, 1H); 4.10 (t, 2H, J=6.5 Hz); 1.80–1.92 (m, 2H); 1.38–1.50 (m, 4H); 0.95 (t, 3H, J=6.9 Hz). IR (KBr, pellet, cm^{-1}): 3074 (br, COOH), 2957, 2930, 2858, 1739, 1685, 1615, 1556, 1503, 1425, 1382, 1256, 1214, 1119, 1002, 970, 873, 820.

*4.3.5 Synthesis of 7-alkoxycoumarin (***E-*n*)*

The preparation procedure of 7-alkoxycoumarin (**E-*n***) is the same as the procedure for preparing **B-*n*** described previously.

Acknowledgements

The authors would like to thank the National Science Foundation Committee of China (Project No. 50802058) and the Youth Foundation of the School of Chemistry and Materials Science, Shaanxi Normal University for financial support of this work.

References

[1] Goodby, J.W.; Mehl, G.H.; Saez, I.M.; Tuffin, R.P.; Mackenzie, G.; Auzely-Velty, R.; Benvegu, T.; Plusquellec, D. *Chem. Commun*. **1998**, *19*, 2057–2070.
[2] Goodby, J.W. In *Handbook of Liquid Crystals*: Demus, D., Goodby, J.W., Gray, G.W., Spiess, H.-W., Vill, V., Eds.; Wiley-VCH: Weinheim, 1998; Vol. 2A, pp 3–21.
[3] Girdziunaite, D.; Tschierske, C.; Novotna, E.; Kresse, H.; Hetzheim, A. *Liq. Cryst*. **1991**, *10*, 397–407.
[4] Zhang, P.; Qu, S.; Wang, H.; Bai, B.; Li, M. *Liq. Cryst*. **2008**, *35*, 389–394.
[5] Qu, S.; Li, M. *Tetrahedron* **2007**, *63*, 12429–12436.
[6] Wen, C.-R.; Wang, Y.-J.; Wang, H.-C.; Sheu, H.-S.; Lee, G.-H.; Lai, C.-K. *Chem. Mater*. **2005**, *17*, 1646–1654.
[7] Lai, C.-K.; Ke, Y.-C.; Su, J.-C.; Lu, C.-S.; Li, W.-R. *Liq. Cryst*. **2002**, *29*, 915–920.
[8] Cristiano, R.; Santos, D.M.P.O.; Gallardo, H., *Liq. Cryst*. **2005**, *32*, 7–14.
[9] Kim, B.G.; Kim, S.; Park, S.Y. *Tetrahedron Lett*. **2001**, *42*, 2697–2699.
[10] Yoshizawa, A.; Yamaguchi, A. *Chem. Commun*. **2002**, *18*, 2060–2061.
[11] Yoshizawa, A.; Kawaguchi, T. *Liq. Cryst*. **2007**, *34*, 177–181.
[12] Yoshizawa, A.; Kinbara, H.; Narumi, T.; Yamaguchi, A.; Dewa, H. *Liq. Cryst*. **2005**, *32*, 1175–1181.
[13] Hurl, S.-M.; Jin, J.-I.; Achard, M.F.; Hardouin, F. *Liq. Cryst*. **1998**, *25*, 285–293.
[14] Sato, M.; Yoshizawa, A. *Adv. Mater. (Weinheim, Ger.)* **2007**, *19*, 4145–4148.

[15] Cristiano, R.; Santos, D.M.P.O.; Conte, G.; Gallardo, H. *Liq. Cryst*. **2006**, *33*, 997–1003.
[16] Gallardo, H.; Bortoluzzi, A.J.; Santos, D.M.P.O. *Liq. Cryst*. **2008**, *35*, 719–725.
[17] Qu, S.; Chen, X.; Shao, X.; Li, F.; Zhang, H.; Wang, H.; Zhang, P.; Yu, Z.; Wu, K.; Wang, Y.; Li, M. *J. Mater. Chem*. **2008**, *18*, 3954–3964.
[18] Kang, S.; Saito, Y.; Watanabe, N.; Tokita, M.; Takanishi, Y.; Takezoe, H.; Watanabe, J. *J. Phys. Chem. B* **2006**, *110*, 5205–5214.;
[19] Reddy, R.A.; Tschierske, C. *J. Mater. Chem*. **2006**, *16*, 907–961.
[20] Gortz, V.; Goodby, J.W. *Chem. Commun*. **2005**, *26*, 3262–3264.
[21] Alderete, J.; Belmar, J.; Parra, M.; Zarraga, M.; Zuniga, C. *Liq. Cryst*. **2008**, *35*, 157–162.
[22] Chudgar, N.K.; Bosco, R.; Shah, S.N. *Liq. Cryst*. **1991**, *10*, 141–145.
[23] Yeap, G.-Y.; Yam, W.-S.; Ito, M.M.; Takahashi, Y.; Nakamura, Y.; Mahmood, W.A.K.; Boey, P.-L.; Hamid, S.A.; Gorecka, E. *Liq. Cryst*. **2007**, *34*, 649–654.
[24] Nakai, H.; Takenaka, S.; Kusabayashi, S. *Bull. Chem. Soc. Jpn* **1983**, *56*, 3571–3577.
[25] Morita, Y.; Kawabe, K.; Zhang, F.; Okamoto, H.; Takenaka, S.; Kita, H. *Chem. Lett*. **2005**, *34*, 1650–1651.
[26] Morita, Y.; Uemura, H.; Shimoi, K.; Kasatani, K.; Okamoto, H. *Mol. Cryst. Liq. Cryst*. **2009**, *508*, 163–172.
[27] Seed, A. *Chem. Soc. Rev*. **2007**, *36*, 2046–2069.
[28] Abd-Allah, O.A. *Farmaco* **2000**, *55*, 641–649.
[29] Vertogen, G.; de Jeu, W.H. *Thermotropic Liquid Crystals*; Springer Verlag: Berlin, 1988.
[30] Gray, G.W. *Molecular Structure and the Properties of Liquid Crystals*; Academic Press: New York, 1962; p 163 and references cited therein.
[31] Creaven, B.S.; Egan, D.A.; Kavanagh, K.; McCann, M.; Noble, A.; Thati, B.; Walsh, M. *Inorg*. *Chim. Acta.* **2006**, *359*, 3976–3984.